Paper 213

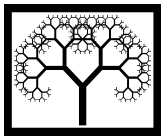

Proceedings of the Seventh International Conference
on Computational Structures Technology,
B.H.V. Topping and C.A. Mota Soares (Editors),
Civil-Comp Press, Stirling, Scotland.

Non-linear FE Analysis of Tension Structures used to Stabilize the External North Façade of Pad 19-20 in the Fiera di Bologna: Comparison of Two Different Proposed Solutions

R. Gori†, M. Majowiecki‡ and A. Mastropasqua†
† Department of Structural and Transportation Engineering
University of Padua, Italy
‡ Department of Construction of Architecture
University IUAV of Venice, Italy

Abstract

This paper describes the tension system solution adopted to stabilize the teflon membrane of the north façade of the Pad 19-20 in Fiera di Bologna (Italy): the authors explain the important structural conditions which have to be taken into account to determine the design pre-stress state of the cable systems of the State 0 condition, and the analytical procedure to find it.

Non-linear geometric analyses results are discussed and some structural problem are highlighted. In particular the influence of the structural border of the tension system on the membrane diplacement is observed: the origin of this effect is investigated and a new tension system solution is proposed to minimize it.

Therefore, for both the systems, the statical responses are shown in order to observe the different behaviour of the membrane under the effect of a wind load: displacement and shape deformation are discussed.

Keywords: tension structures, membrane, cables, pre-tension, non-linear analysis, state 0.

1 Introduction

Pad 19-20 of "Fiera di Bologna" (Italy) (Figure 1) is an example of a recent application of a tensioned structure where the structure itself is more than simply a link between two distant points. Here the tension structure is an important part of the global structural concept. It is utilized in the roof and north external facade.

On the roof, the tension system has been used with compression members in an unusual high span truss system. The north façade system consists of a 1070 m^2 Teflon fabric envelope and 15 uniformly spaced (every 4 m) and pre-tensioned rope systems (following called cable-beams). Here the tension structure has been used as an efficient and ingenious medium to provide stability under wind and lateral loads.

This paper addresses the principal strategies that led to the actual structural solutions. That of a pre-tensioned net cable system and of that presented by the 15 independent pre-tensioned cable-beams. Both solutions have been calculated by Finite Element Analysis, taking into account the problems inherent in finding "State 0", and the problem related to defining the influence of border structures on the static and dynamic response in the facade system. Those results have been obtained with the help of a non-linear Finite Element Analysis solver that utilizes the non-linear material of "only tension members" called Cutoff Bars and implements the non-linear geometric behaviour of the fabric and pre-tensioned tension systems. The resulting solutions have been compared, their differences highlighted, and analogies between them drawn.

Figure 1: Pad 19-20 in Fiera di Bologna.

The hanging structure of the north façade (Figures 3,4) is comprised of two concrete columns supporting two beams. The top is a composite beam (n° 2 HE1000 coupled by secondary transversal steel elements) and the lower is comprised of a single profile type HE1600. The latter element is positioned with its intrados at 4479 mm above grade. The two meter high tubular steel structure that bears the glass structure is welded to the extrados. The beams are connected each other by a columns system (8 steel columns, 4 outside and 4 inside the building).

The columns have rectangular hollow cross-sections which vary in size along their length. The whole system is suspended by twelve D42 post tensioned spiral ropes. The lower beam ultimately being supported at four points, the interior two being flexible with respect to the D42 rope system stiffness.

Figure 2: Pad 19-20: north façade.

The upper beam, with parabolic trajectory and low curvature, is supported at six points with two fixed members (the externals), and four flexible members (internals): the flexibility being determined by the stiffness of the whole lower mechanical system (lower horizontal beam + 8 RHS colums + D42 rope system structural response). Note how all the external members are vertically fixed, demonstrated by the negligible vertical displacements of the concrete system. With regard to horizontal displacements, the designer incorporated an elastic spring system to take into account the horizontal displacement due the thermal loads on the lower beam and thermal loads plus horizontal end-arch displacement due the arch vertical deflection under external load. The lower members utilize a simple Neoprene springs. For the upper attachments a special linear spring system with a fixed elastic linear stiffness of X = 1 kN/mm and maximum 20 mm slide capacity was developed. Two elastic spring systems are present: one for each end-arch (see Figure 3):

Figure 3: Upper arch-beams view.

As a result of the many stabilizing elements connecting the steel frame to the concrete frame and the rest of the structure, the static restraint scheme is hyperstatic in the vertical direction Z, isostatic in the horizontal direction X (parallel to the longitudinal lower beam axis), and hyperstatic in the normal façade direction Y.

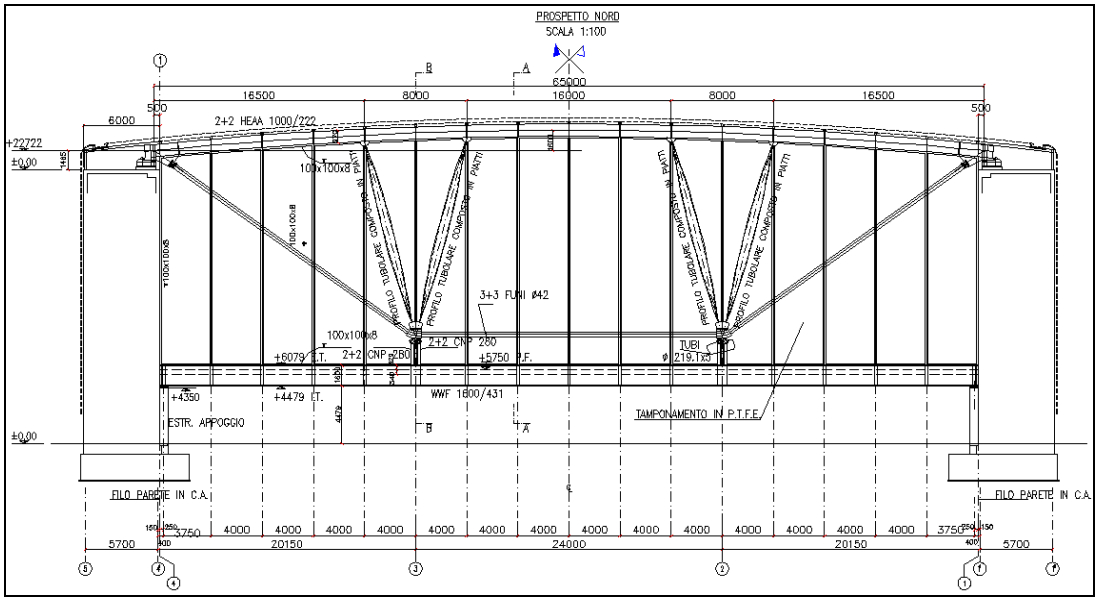

Figure 4: Frontal view of north façade (extracted from executive drawing)

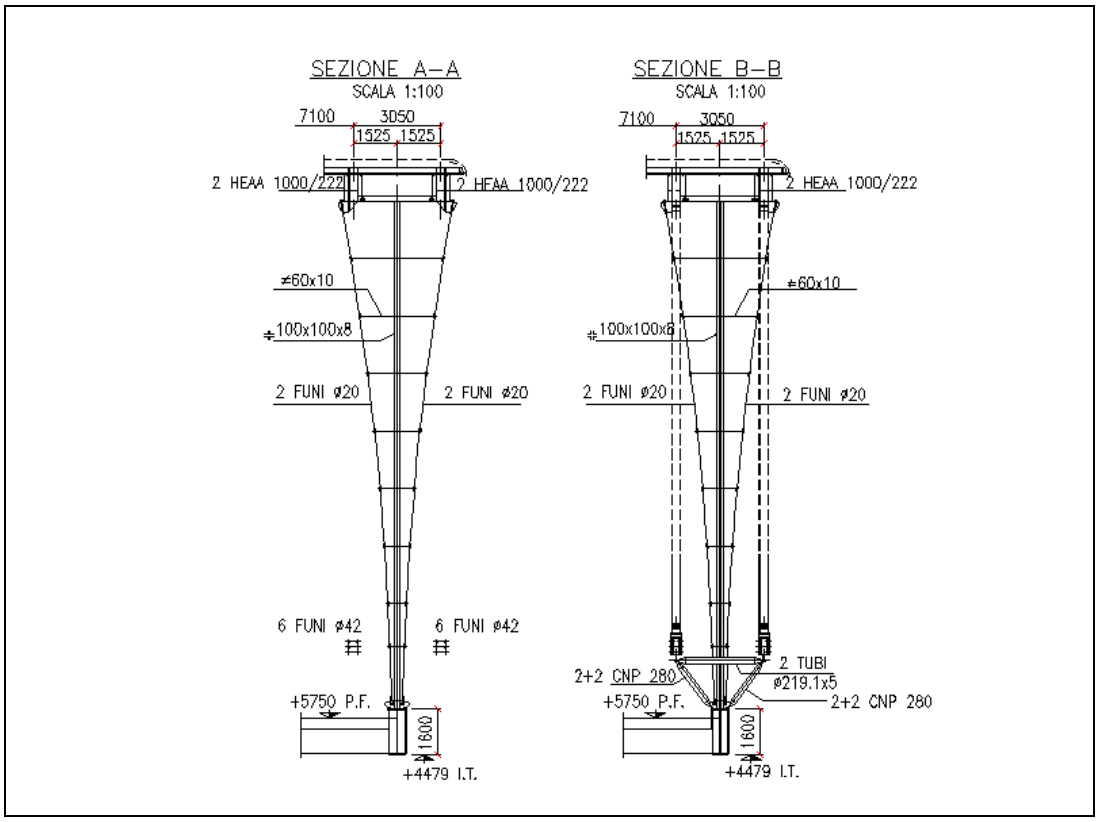

Figure 5: Typical section of D20 pre-tensioned cable systems
(extracted from executive drawing)

2 The F.E. modelling

2.1 Cable element representation

It has been represented using 'cut-off bar' finite elements, without shear and bending stiffness and with an assigned tension range. As a result no elements were compressed during every iteration. The cable stiffness matrix for a general element (e) in a polar coordinate system with α and β values for angles [1][2], appears in Figure 6.

$$K^{(e)} = \begin{bmatrix} [(EA-N)\cos^2(\alpha)+N]/L & (EA-N)\cos(\alpha)\operatorname{sen}(\alpha)/L & (EA-N)\cos(\beta)\cos(\beta)/L & -[(EA-N)\cos^2(\alpha)+N]/L & -(EA-N)\cos(\alpha)\operatorname{sen}(\alpha)/L & -(EA-N)\cos(\alpha)\cos(\beta)/L \\ (EA-N)\cos(\alpha)\operatorname{sen}(\alpha)/L & [(EA-N)\operatorname{sen}^2(\alpha)+N]/L & (EA-N)\operatorname{sen}(\alpha)\cos(\beta)/L & -(EA-N)\cos(\alpha)\operatorname{sen}(\alpha)/L & -[(EA-N)\operatorname{sen}^2(\alpha)+N]/L & -(EA-N)\operatorname{sen}(\alpha)\cos(\beta)/L \\ (EA-N)\cos(\alpha)\cos(\beta)/L & (EA-N)\operatorname{sen}(\alpha)\cos(\beta)/L & [(EA-N)\cos^2(\beta)+N]/L & -(EA-N)\cos(\alpha)\cos(\beta)/L & -(EA-N)\operatorname{sen}(\alpha)\cos(\beta)/L & -[(EA-N)\cos^2(\beta)+N]/L \\ -[(EA-N)\cos^2(\alpha)+N]/L & -(EA-N)\cos(\alpha)\operatorname{sen}(\alpha)/L & -(EA-N)\cos(\alpha)\cos(\beta)/L & [(EA-N)\cos^2(\alpha)+N]/L & (EA-N)\cos(\alpha)\operatorname{sen}(\alpha)/L & (EA-N)\cos(\alpha)\cos(\beta)/L \\ -(EA-N)\cos(\alpha)\operatorname{sen}(\alpha)/L & -[(EA-N)\operatorname{sen}^2(\alpha)+N]/L & -(EA-N)\operatorname{sen}(\alpha)\cos(\beta)/L & (EA-N)\cos(\alpha)\operatorname{sen}(\alpha)/L & [(EA-N)\operatorname{sen}^2(\alpha)+N]/L & (EA-N)\operatorname{sen}(\alpha)\cos(\beta)/L \\ -(EA-N)\cos(\alpha)\cos(\beta)/L & -(EA-N)\operatorname{sen}(\alpha)\cos(\beta)/L & -[(EA-N)\cos^2(\beta)+N]/L & (EA-N)\cos(\alpha)\cos(\beta)/L & (EA-N)\operatorname{sen}(\alpha)\cos(\beta)/L & [(EA-N)\cos^2(\beta)+N]/L \end{bmatrix}$$

Figure 6: Cable element stiffness matrix

where for each element we assumed:

EA = 40400 kN	(axial stiffness)
MBF = 380 kN	(minimum breaking force)
L = 412/2070 mm	(minimum and maximum length)

Notes (Figure 6), the dependence of the stiffness terms:

1. from the invariancy of section mechanical properties (EA)
2. from the variancy of the instant geometric configuration (α , β)
3. from the variancy of section state stress (N)

2.2 Cable-beam hypostaticity

The use of a line of cut-off bar elements (by series) lead to a high number of hypostatic sub-models, and then to many singularities in the linear global stiffness matrix (det $K_0 = 0$). For this reason numerical processing of the rigid parts of the structure [3][4] wasn't possible. The numerical problems related to the hypostatic sub models can be seen by presenting the extraction and assembly procedure of stiffness matrix for the general (e) finite element and then showing the internal potential energy expression for an element with twelve degrees of freedom[3][5]:

$$\Pi_i = \tfrac{1}{2} \int (\varepsilon^T \cdot \sigma)\, dx\, dy\, dz = \tfrac{1}{2} \int (\varepsilon + \Delta\varepsilon)^T \cdot (\sigma + \Delta\sigma)\, dx\, dy\, dz \qquad (1)$$

Where the 3rd part of the equation has been written considering the update of nodals coordinates, with reference to a particolar initial geometric and stress configuration. Now, making explicit the corresponding vector [6]:

$\varepsilon = (\varepsilon_3 , \gamma_{23}, , \gamma_{13})^T$ (2) and $\sigma = (\sigma_3 , \tau_{23}, , \tau_{13})^T$ (3) we obtain :

$$\Pi_i = \tfrac{1}{2} \int (\varepsilon^T \bullet \sigma)\, dx\, dy\, dz + \tfrac{1}{2} \int (\varepsilon^T \bullet \Delta\sigma)\, dx\, dy\, dz + \tfrac{1}{2} \int (\Delta\varepsilon^T \bullet \sigma)\, dx\, dy\, dz + \tfrac{1}{2} \int (\Delta\varepsilon^T \bullet \Delta\sigma)\, dx\, dy\, dz \qquad (4)$$

and, filling in (4) the material elastic relationship (2) e (3) we can write:

$$\Pi_i = \tfrac{1}{2} \int (\varepsilon^T \bullet E \bullet \varepsilon)\, dx\, dy\, dz + \tfrac{1}{2} \int (\varepsilon^T \bullet E \bullet \Delta\varepsilon)\, dx\, dy\, dz + \tfrac{1}{2} \int (\Delta\varepsilon^T \bullet E \bullet \varepsilon)\, dx\, dy\, dz + \tfrac{1}{2} \int (\Delta\varepsilon^T \bullet E \bullet \Delta\varepsilon)\, dx\, dy\, dz \qquad (5)$$

grouping together the terms of the 2nd part of the equation (5), 3 energetic factors can be highlighted [3][4]:

$$\Pi_{i1} = \tfrac{1}{2} \int (\varepsilon^T \bullet E \bullet \varepsilon)\, dx\, dy\, dz \qquad (6)$$

$$\Pi_{i2} = \tfrac{1}{2} \int \varepsilon^T \bullet E \bullet \Delta\varepsilon\, dx\, dy\, dz + \tfrac{1}{2} \int \Delta\varepsilon^T \bullet E \bullet \Delta\varepsilon\, dx\, dy\, dz \qquad (7)$$

$$\Pi_{i3} = \tfrac{1}{2} \int \Delta\varepsilon^T \bullet E \bullet \varepsilon\, dx\, dy\, dz \qquad (8)$$

where :

Π_{i1} (eq. 6) represents that component of internal potential energy due to the initial geometric and stress configuration

Π_{i2} (eq. 7) represents that component of internal potential energy due to the updating of the stress state

Π_{i3} (eq. 8) represents that component of internal potential energy due to the updating of the geometric state

Now, for double differentiation of (6), (7), (8) on the geometric displacements variable (Lagrange coordinates q_i) we obtain the terms of the global stiffness matrix:

$$\partial^2\Pi_{i1} / \partial q_i^2 = k_{0i} \quad \text{assembled term of initial linear stiffness matrix } (K_0) \tag{9}$$

$$\partial^2\Pi_{i2} / \partial q_i^2 = k_{Gi} \quad \text{assembled term of non-linear stress stiffening matrix } (K_G) \tag{10}$$

$$\partial^2\Pi_{i3} / \partial q_i^2 = k_{\theta i} \quad \text{assembled term of non-linear geometric stiffness } (K_\theta) \tag{11}$$

the contributions of the non-linear terms (10) and (11) annul the singularities of the global stiffness matrix ($K= K_0 + K_G + K_\theta$). Note how, at the 1rst iteration, the non-linear geometric stiffness matrix (K_θ) is singular because no strain (ε) and no variation of strain ($\Delta\ \varepsilon^T$) are definable [7]. Unable to bypass the numerical singularity problem: its implementation was necessary to calculate the 2nd sort of non-linear term from stress stiffening matrix (K_G). This matrix has, unlike those the matrix K_θ , the det (K_G)$\neq$0 already at the beginning of the 1rst iteration, when the global stiffnes matrix is assembled. It follows that the 'start solution' procedure by Newton-Rapshon was permitted and, for the successive iterations, updates of the global matrix (K) occurred by (10) and (11).

The final non-linear numeric equation system can then be represented as:

$$K_0 \bullet U = -P + R_{NL}(q) \tag{12}$$

where:
U is the unknown nodal displacements vector
P is the nodal equivalent external forces vector
$R_{NL}(q)= [K_G + K_\theta] \bullet U$ is the geometric and stress stiffening non-linear vector, depending on Lagrange coordinates (q)

3 The search of "State 0"

We know from the "Tension Structures Theory" that the State 0 is the geometric and stress configuration relative to the action of structural dead load and assigned pre-stress [3]. Further we define State 1 the same configuration where the action of

permanent dead load is also involved. In this article, in order to highlight the importance of the geometric configuration, and in order to conform the treatment to most of the specialized texts [3][8][9][10][13][15], we will consider the structural deal load, permanent dead load and assigned pre-stress configuration, calling this configuration State 0. State 0 configuration has been reached by defining two particular structural parameters:

- the pre-tension state of D42 OSS (Open Spiral Strand), which belongs to the principal steel structure
- the pre-tension state of D20 OSS (Open Spiral Strand), which belongs to the façade tension system

Finding the solution, the State 0 must satisfy the following conditions:

Condition n° 1: Lower beam (type HE1600) horizontality.

Its influence is fundamentally in defining the Z dimension where the HE1600 beam is linked to the D42 OSS cable (Figure 7) in this way we ensure that the HE1600 beam remains horizontal.

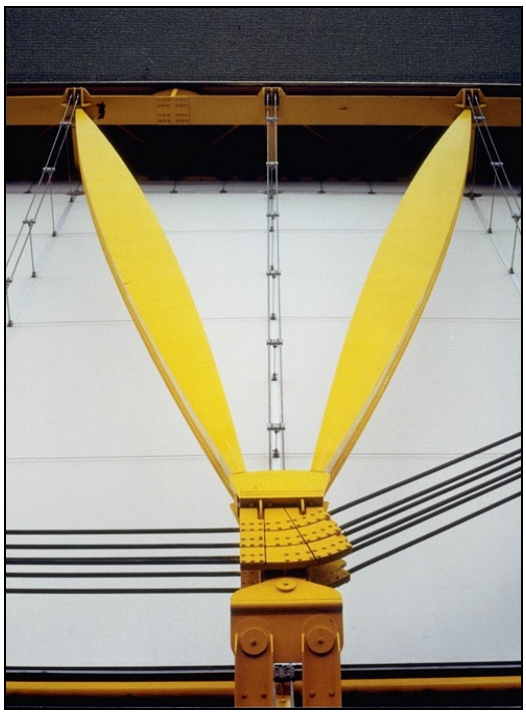

Figure 7: Double trilateral system linking: columns-D42 ropes-HE1600

Condition n° 2: Torsional rotation of beam HE1600.

The considerable length of the beam HE1600 (63500 mm) and the action of dead and permanent load of the beams HE900A constitute the internal loft and cause the HE1600 beam to rotate around its longitudinal axis. Numerical analysis shows a deflection angle δ=2.23°deg relative to the State 0 configuration. In order to recover

this angle, we subdivide this amount of rotation in two parts δ_1= 1.4°deg δ_2=0.83°deg so that $\delta = \delta_1 + \delta_2$. The 1^{rst} angular displacement δ_1=1.4°deg was annulled by pre-tensioning the external and the internal D42 OSS with different loads, creating two concentrated applied torques on the HE1600. The static effect on the beam was critically studied to observe the stress state resulting from the concentrate torques. Figure 8 shows the effect of the different pre-tension load applied on the lower beam.

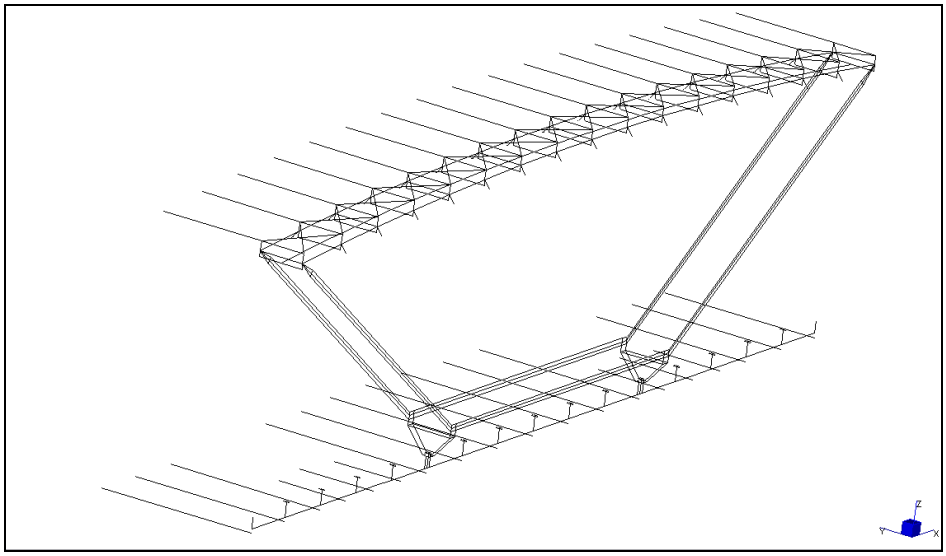

Figure 8: Lower system D42 ropes-HE1600 beam

The 2nd angular displacement δ_2=0.83°deg was corrected during the installation procedure, impressing an opportune angular displacement of δ_{2opp}= -0.80°deg to the double trilateral system visible in Figure 7 and Figure 8. This rotation corresponded to a linear displacement of 27 mm on the top (extrados) of HE1600.

Condition n° 3: Allowable load and stability of cables.

For 'allowable load' we intended the maximum tension reached from every cut-off bar finite element at the end of each load increment [3] for the D42 OSS and D20 OSS cable elements. Although the maximum breake tension, certified by the rope manufacturer (Tensoteci s.p.a.- Italy), is the MBF (Minimum Breaking Force), as usual for the tension structures, we assumed the following limits:

-MT_0 : maximum tension at State 0: it corresponds to 32% of MBF
-$MT_{2/3}$: maximum tension at State 2/State 3: it corresponds at the worst combination case where the cables reaches the maximum absolute tension value or/and the minimum absolute tension value. For both the situations we checked these values, ensuring they always result less of 52% MBF and more of 8% MBF.

The maximum allowable load (52% MBF) depends on the safety load design factor of the ropes, taking into account the safety factor:

- of the single wire
- of the whole cable
- of the end fork terminal

The minimum allowable load (8% MBF) comes from the requirement to have, for any combination case, every cable element with a minimum residue pre-tension [3], in order to ensure a minimum stiffness of the system at which the cable belongs. In particular must avoid the vibration problem in tension structures.

Condition n° 4 : Membrane displacement

For each combination case, the horizontal displacements of the teflon-fabric have been checked.

4 The Functional problem

Now we can enunciate the analytical procedure used to find the State 0 configuration [3][8][9]. Defining the total potential energy of a beam under an axial stress state, and supposing a general initial pre-stress ($\sigma°$) (for example we could suppose the pre-stress related the State 0) , we can write:

$$\Pi_T^0 = \Sigma_{i=1}^m \; ½ \int (\sigma_i^0 \, \varepsilon_i^0)\, dv + D_n^t \cdot P_n^0 = \Sigma_{i=1}^m \; ½ \, S_i^0 \, (l_i - l_i^0) + D_n^t \cdot P_n^0 \qquad (13)$$

where:

σ_i^0 = initial pre-stress of general i-cable
ε_i^0 = initial pre-strain of general i-cable
D_n = global displacement vector
P_n^0 = external nodal State 0 force vector
Π_T^0 = total potential energy at State 0 configuration, where the 1^{rst} (first) integral member represents the external potential energy

Furthermore we need the following external conditions, where some of them have been above explained (Conditions n° 1,2,3,4) [3]:

$$\varphi_1(x,y,z) = 0 \;\text{ thus }\; [(x-x^0)(y-y^0)(z-z^0)]_k^t \;\text{ (initial configuration condition)} \qquad (14)$$

with x^0, y^0, z^0 assigned geometric coordinates of generic k-node at State 0

$$\varphi_2(x,y,z) = 0 \;\text{ thus }\; l^0_{k,k+1} - \underline{l}^0_{k,k+1} = 0 \qquad \text{(cable length condition)} \qquad (15)$$

with $\underline{l}^0_{k,k+1}$ = assigned initial length of generic cut-off bar element between the nodes k and k+1

$$\varphi_3(x,y,z) = 0 \;\text{ thus }\; S^0_{k,k+1} - \underline{S}^0_{k,k+1} = 0 \qquad \text{(allowable load cable condition)} \qquad (16)$$

with $\underline{S}^0_{k,k+1}$ = assigned limit value for the cut-off bar element between the nodes k and k+1

The solution can be obtained by the minimization of the total potential energy and the simultaneous verification of the external conditions, so that, defined a potential Φ, we have:

$$\partial\Phi/\partial x_1 = \partial\Phi/\partial y_1 = \partial\Phi/\partial z_1 = \partial\Phi/\partial x_2 = \partial\Phi/\partial y_2 = \partial\Phi/\partial z_2 = \ldots = \partial\Phi/\partial z_n = 0 \qquad (17)$$

where

$$\Phi(x_1,y_1,z_1, \ldots, x_n,y_n,z_n) = \Pi_T{}^0(x,y,z,S) + \Sigma j_{=1}{}^r \lambda_j \varphi_j(x,y,z,S) \qquad (18)$$

is the Lagrange expression of the associated function [5].

The solution searching procedure had touched 3 points:

Phase 1: Determination of D42 OSS pre-tension in order to verify to n°1, n°2, n°3 conditions above (horizontal position of HE1600 beam, torsional rotation of HE1600, allowable strand load).

Phase 2: Determination of D20 OSS pre-tension in order to verify the n°3 and n° 4 conditions (façade stabilization, allowable strand load).

Where completion of the Phase 2, resulted in a non-optimum solution, Phase 1 was reiterated. Therefore, in order to verify both phases and produce an optimal solution an iterative numerical procedure has been followed (Phase1 → Phase2 → Phase1 → Phase2 → Phase1 →...). This iterative procedure has been called Phase 3. Phase 3 terminated when both Phase 1 and Phase 2 became verifiable and optimised simultaneously. At the end of Phase 3, the D20 OSS pre-stress state configuration resulted as in Figure 9:

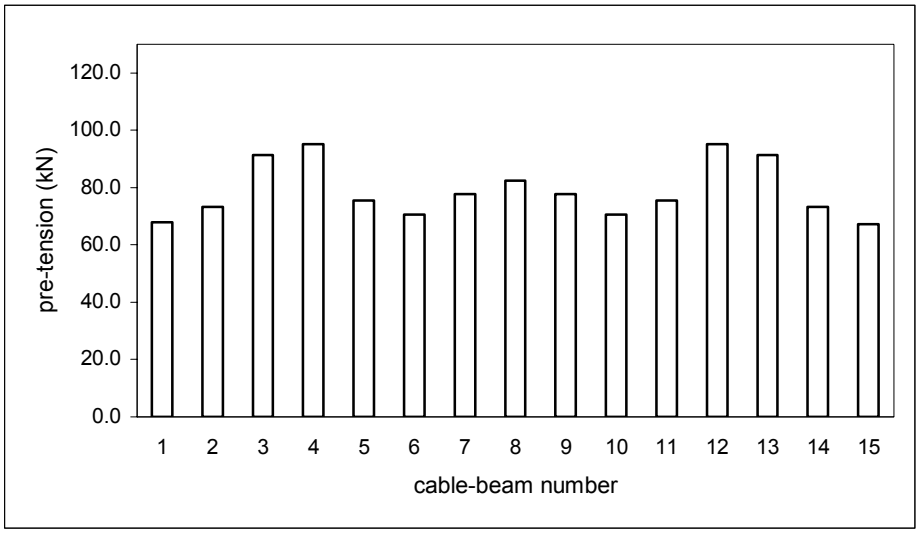

Figure 9: Pre-tension distribution (average value) for the 15 cable-beam system

Note the irregular pre-tension corresponding to the cable-beam system n°3 and n°4 (and their symmetrical n°12 , n°13). Detail are exposed in the paragraph n°5.

5 Result analysis: the influence of the border on the displacement

The membrane behaviour has been studied by a series of vertical and horizontal sections. Contour displacements are also represented.

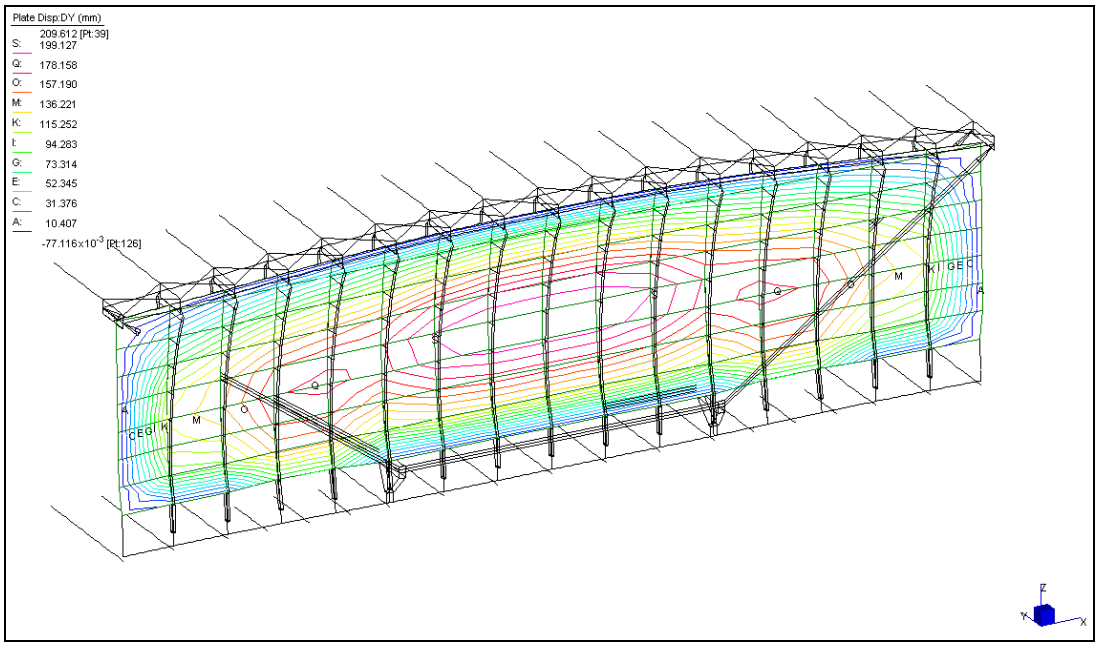

Figure10: Wind load: horizontal displacement

Note how the deformation of the membrane is different from the pseudo-paraboloidical shape, correct for a rectangular membrane under the effect of a normal pressure and with ideal edge restraint (cylindrical edge pin). A study of the following diagrams (horizontal sections) highlights the origin of this phenomenon: a dependency on the HE1600 torsional stiffness reduction due to the irregular disposition of the loft beams HE900A. With the exception of cable-beam n° 3 and n° 4, the loft beam HE900A is attached to the HE1600 by regular step lengths.

This is more clearly visible in Figure 11, which shows the horizontal displacement of the lower half of the façade at four different levels: from Level 0 (low border of membrane) to Level 3 (mid section of façade).

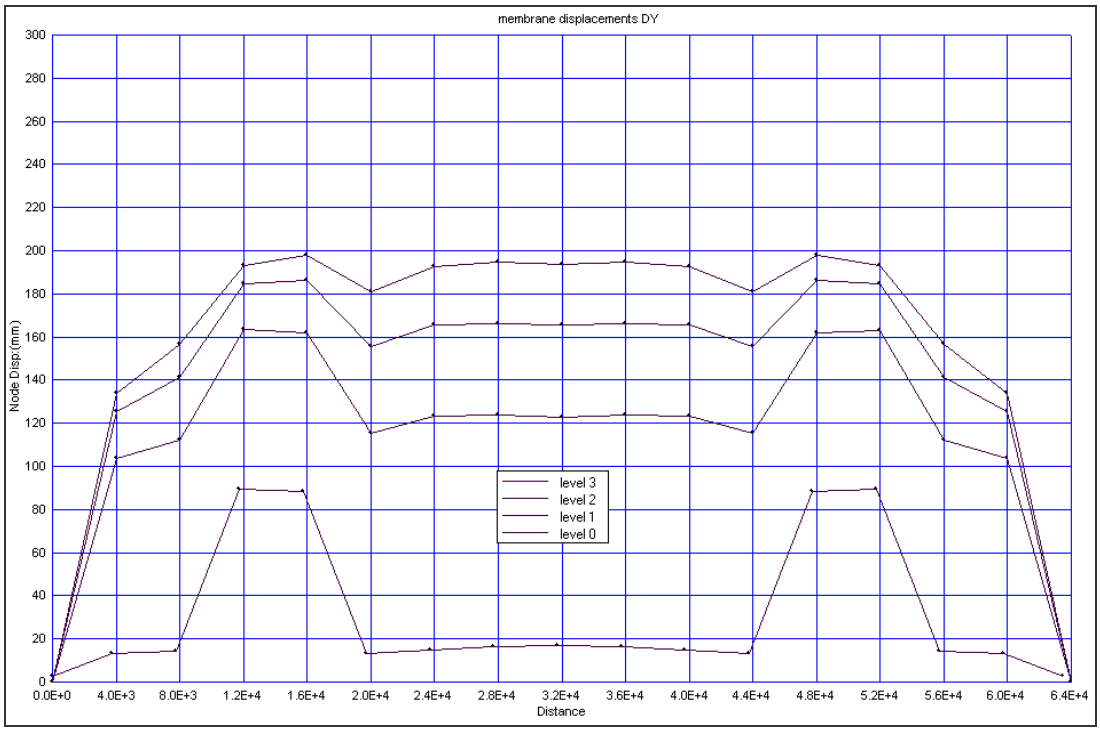

Figure 11: Wind load: horizontal displacement by horizontal sections

We can note the initial displacements at the cable-beam n° 3 and n° 4 (and their symmetrical). These displacements depend on a torsional rotation of the section HE1600 around its longitudinal axis. This rotation influences the whole membrane displacement in the lower level, while its effect decreases towards the upper zone of the façade. This result leads to an assessment and deep study of the influence of the border on the tension system [9][10][11], particularly that of the pre-tension state of n° 3 and n° 4 D20 OSS cable-beam. It was furthermore necessary take into account the study of a different tension system capable of reducing or nullifying the problem of HE1600 torsional rotation. It was not possible the modification of the step length of the HE900A loft beams because of the fixed internal structure.

An alternative solution studied, capable of reducing the problem, but not eliminate it, is to incorporate a D24 OSS cable-net system with 2m x 2m step cable mesh. The model is visible in Figure 12:

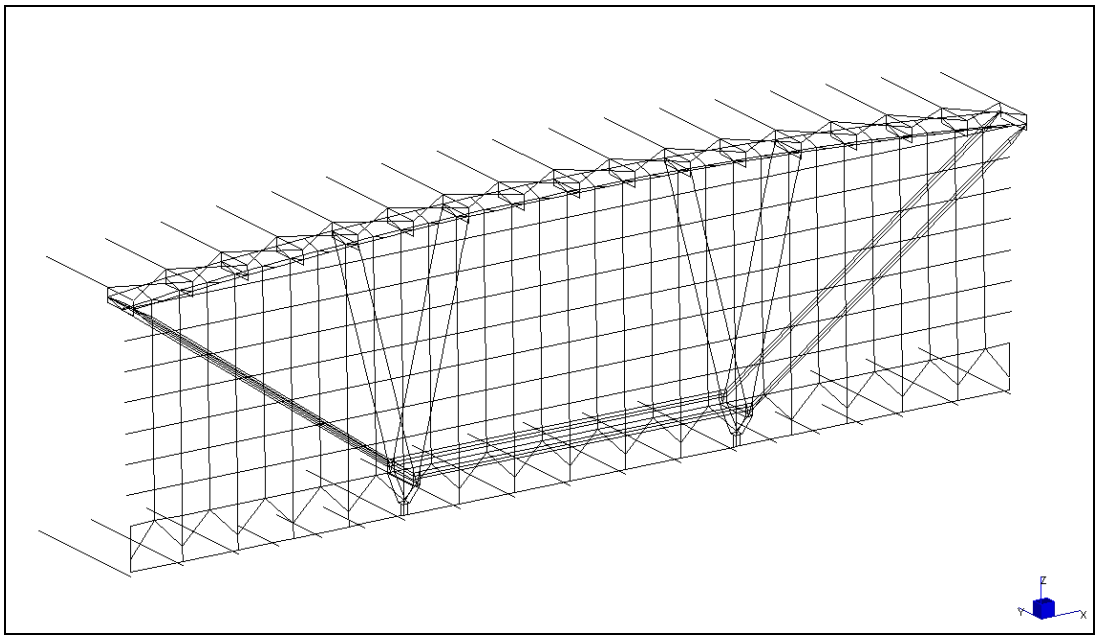

Figure 12: Cable-net tension system (2m x 2m cable mesh)

As in the previous finite element model (cable-beams) we show the D24 OSS pre-tension state reached at State 0 in Figure 13, the horizontal displacement of the membrane by a contour displacement in Figure 14, and by horizontal sections in Figure 15.

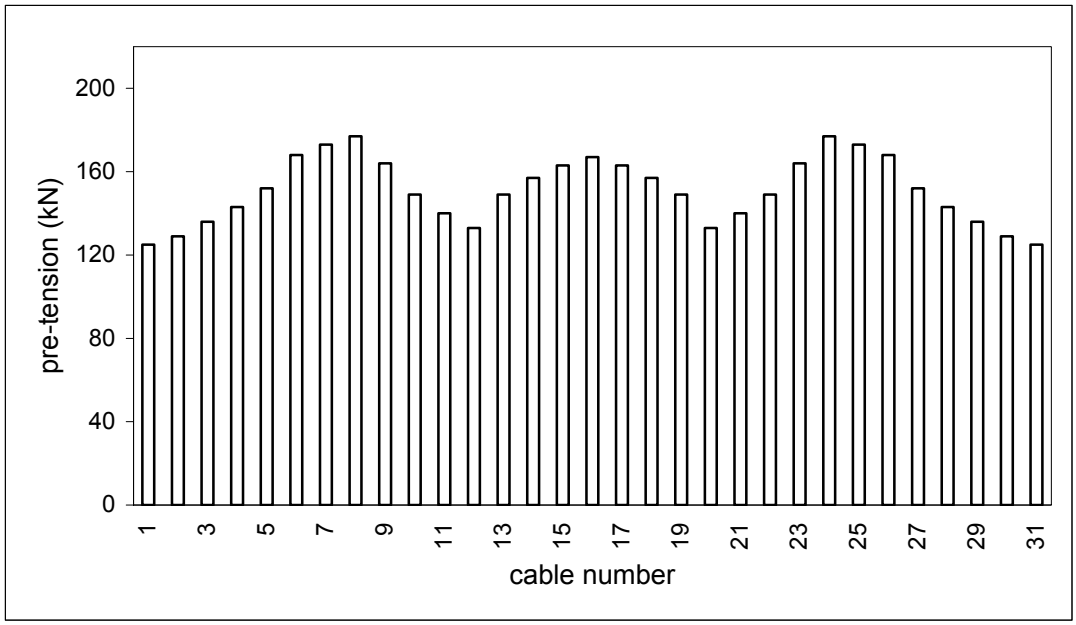

Figure13: D24 pre-tension state at State 0 for vertical cable.

For the horizontal cables we supposed instead a constant pre-tension of 140 kN

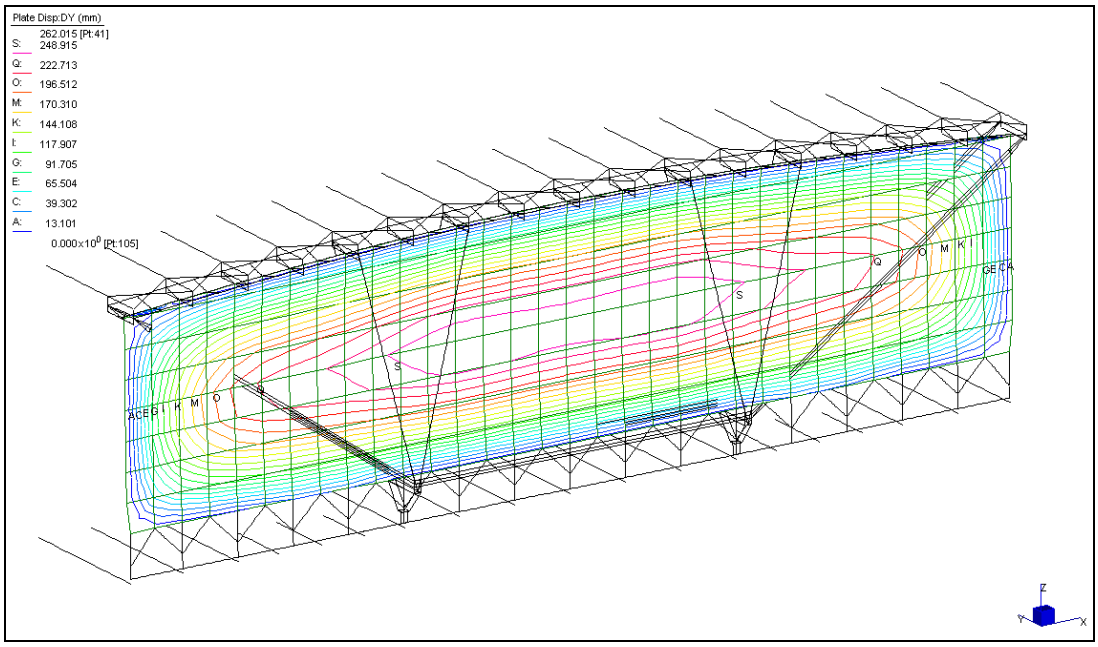

Figure 14: Wind load: horizontal displacements

Observing the iso-displacement curves on Figure 14 we note the different displacement shape of the membrane; this geometric configuration is closer to a pseudo-paraboloidical shape. Nevertheless a greater horizontal displacement at the centre point of the membrane (31% greater) was obtained.

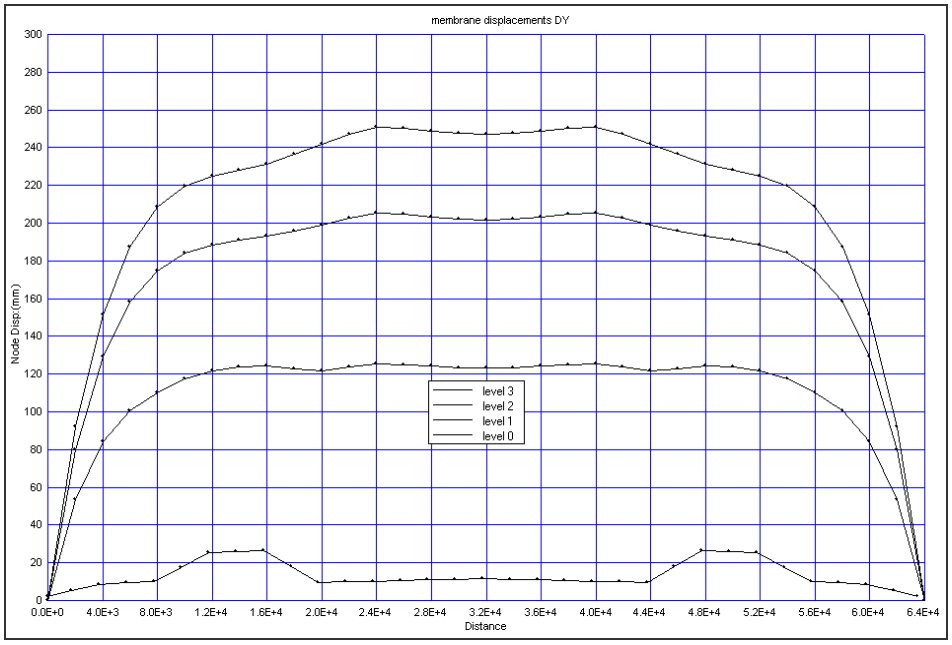

Figure 15: Wind load: horizontal displacement by horizontal sections

At the end of the comparison we note (Figure 15) a clear reduction of the 'initial displacement' at Level 0 with respect to the cable-beams structural model, and a more regular trend of the membrane displacements at each section level.

6 Conclusions

The numerical comparison between the two structural models leads to some observations which influence the choice of the most rational tension system solution to be adopted for the façade:

6.1 Tension system stiffness

Analysing the displacement of the membrane under the effect of the wind load, we observe that the cable-beams system, thanks to its characteristic V shape, provides the best structural response. In particular, the V shape provides an initial rigidity without any initial displacement. Whereas, the cable-net system must reach an initial paraboloidic configuration to give its stiffness. This is clear considering the negligible curvature the cable-net has under no one load. The cable-net needs to deforms itself before to increase its stiffness according to its typical load-displacement hardening relationship.

6.2 Type of statical response

Between the two models there is an important difference about the localization of the displacement. The cable-beam system has an independent response for each cable-beam, while the cable-net system provides a global behaviour similar to a continuous membrane.

6.3 Pre-tension load amount

Although the two systems have the same vertical load resultant, the cable-net system needs the pre-tension of the horizontal cable field (140 kN/each). It leads to a more rigid border structures (particularly on the two lateral concrete structures).

6.4 Dynamic response

Besides highlighting the greater sensibility of the vibration of the cable-beams system with respect to the cable-net system (see" Type of statical response"), no single common problem arose for both solutions. Both the solutions have a positive dynamic response for natural frequencies analysis and dynamic wind/seismic analyses. This analysis has been conducted considering all the masses and the stress state of State 0.

References

[1] E.Viola: Fondamenti di analisi matriciale delle strutture (Pitagora Editrice, Bologna, 1996)

[2] G.Bolzon, A.Saetta, C.Majorana, R.Vitaliani: Lezioni di Calcolo Automatico (CUSL, Padova,1994)

[3] M.Majowiecki: Tensostrutture: Progetto e Verifica (Edizioni Crea,1994)

[4] E M.A.Crisfield: Non-linear Finite Element Analysis of Solids and Structures (J.Wiley & Sons, 1999)

[5] G.Gambolati: Metodi Numerici (Edizioni Libreria Cortina, Padova, 1994)

[6] O.C.Zienkiewicz, R.L.Taylor: The Finite Element Method (McGraw Hill, 1991)

[7] J.Michalos, C.Birnstiel: Movements of a cable due to changes in loading (ASCE ST12, 1960)

[8] M.Majowiecki, G.Tironi: Geometrical configuration of pneumatic and tent structures obtained with CAD (IASS World Congress on Space Enclosures-Wcode, Montreal, 1977)

[9] S.Odorizzi, B.Shrefler: Contributo allo studio di reti di funi pretese entro strutture elasticamente deformabili (Costruzioni Metalliche n°3, 1974)

[10] M.Majowiecki, F.Zoulas: On the elastic interation between rope net and space frame anchorage structures (Third International Conference on Space Structures - University of Surrey - Guilford, 1985)

[11] K.Ishii: Structural design of cable-reinforced membrane structures (IASS World Congress- Madrid, 1989)

[12] G.Diana, F.Cheli: Dinamica e Vibrazione dei Sistemi (Utet Libreria, 1993)

[13] F.Matildi, C.Foti: Tensostrutture e Sistemi Reticolari Spaziali (Italsider, Genova, 1971)

[14] L.Grunding, J.Bahndorf: Form finding of a roof structures for a health Spa Light Structures in Architecture (IASS World Congress- Madrid, 1989)

[15] M.Cannarozzi: Un procedimento di ricerca di forma per reti di funi (ISCB, Bologna, 1979)

[16] M.Majowiecki, G.Tironi: Alcune applicazioni di progettazione interattiva mediante calcolatore nello studio di strutture fortemente deformabili (INAR, Bologna, 1978)